Title

Atomic Resolution Imaging of Light Elements in a Crystalline Environment using Dynamic Hollow-Cone Illumination Transmission Electron Microscopy

Journal

Microscopy and Microanalysis, 26(4)

ISSN

1431-9276

Authors

Brown, Hamish G

Ciston, Jim

Publication Date

2020-08-01

DOI

10.1017/s1431927620001658

Peer reviewed

Atomic resolution imaging of light elements in a crystalline environment using dynamic hollow-cone illumination transmission electron microscopy

Hamish G. Brown, Jim Ciston

April 15, 2020

Abstract

Multiple electron scattering and the non-intuitive nature of image formation with coherent radiation complicates interpretation of conventional transmission electron microscopy (CTEM) images. Precession of the illuminating beam in TEM can lead to more robust and interpretable images with some penalty to image contrast, a technique known as dynamic hollow-cone illumination TEM. We demonstrate direct and robust imaging of light and heavy atoms in a crystalline environment with this technique. This method is similar to the annular bright-field technique in scanning transmission electron microscopy, via the principle of reciprocity. Dynamic hollow-cone illumination TEM is challenging in practice due to sensitivity to the misalignment of the precession axis, microscope objective aperture and crystal zone axis.

1 Introduction

Transmission electron microscopy (TEM) is an invaluable tool in materials science and biology because of its ability to produce sub-Ångstrom resolution images of very small volumes of material. A TEM is typically operated in one of two modes. In conventional transmission electron microscopy (CTEM), plane wave illumination is used and an image of the electron wave can be formed with a post specimen lens. In scanning transmission electron microscopy (STEM) an image is typically formed using signal recorded by a post-specimen diffraction plane detector as a function of the position of a raster-scanned focused electron probe. Broadly speaking, CTEM is favoured for beam sensitive materials, particularly biological samples, due to it being relatively straightforward ability to produce phase contrast through a slight defocus of the imaging lens (Henderson, 1995) enabling superior signal to noise for most thin and weakly scattering specimens (Rez, 2003). Since the whole region of interest is illuminated simultaneously in CTEM this technique is usually preferred for in-situ work since the acquisition time is not limited by the speed of the probe raster scan. Conversely STEM is typically favoured for studies of strongly scattering crystalline materials where more directly interpretable images are required. Common STEM methods include the use of a high-angle annular dark-field (HAADF) detector, in which column intensity approximately scales as a function of the square of atomic number Z^2 (Pennycook & Boatner, 1988) and thickness of the atomic column, or an the use of an annular bright-field (ABF) detector (Findlay et al., 2009, 2010), where both light and heavy atoms can be revealed as dark contrast on a white background if the probe is focussed on the upper-most surface of the specimen. Images of even thin crystalline specimens in CTEM can be difficult to interpret since multiple scattering of the electron beam coupled with the often confounding behaviour of the TEM lens contrast transfer function (CTF) means that there is no simple relationship between, for example, image contrast and atomic number. Additionally imaging crystal lattices with the high coherence sources available in a modern TEM leads to unintuitive results. A periodic crystal lattice will appear to have no obvious plane of focus for maximum interpretability in a TEM as the electron wave scattered from the different atomic sites will alternately constructively and destructively interfere at different image planes (Cowley & Moodie, 1957). At each of these focal planes the relationship between the positions of the columns apparent in the image and the actual positions of columns in the crystal unit cell is typically ambiguous (Spence, 2013).

An imaging mode that preserves the benefits of CTEM imaging, most importantly simultaneous image acquisition over a large field of view, whilst introducing some benefits of STEM imaging modes, such as more directly interpretable column contrast and a single point of focus, would thus be useful. In this paper we consider an approach to making CTEM images of crystals more interpretable by precession of the plane wave illumination in a hollow-cone geometry during imaging. This technique is typically referred to as dynamic-hollow-cone illumination (DHCI) TEM – a nomenclature that we adopt here for consistency with previous literature. Averaging over the different illumination tilt angles through precession (Kunath et al., 1985; Sidorov et al., 2000; Rebled et al., 2011), using a static hollow-cone objective aperture (Saxton et al., 1978) or simply by excitation of a diverging prefield lens (Nagata et al., 1976) has already been demonstrated to result in

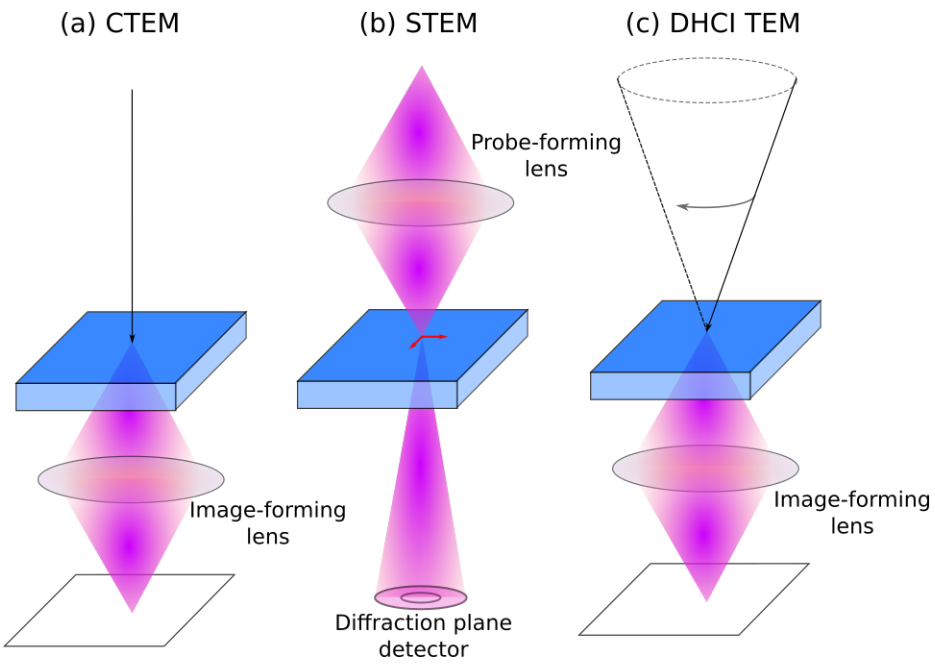

Figure 1: A diagram of the main techniques discussed. (a) Conventional transmission electron microscopy (CTEM) where a post-specimen lens forms an image of the transmitted plane-wave illumination. (b) Scanning trnasmission electron microscopy (STEM) where a focused probe is rastered across the sample and the signal in a post-specimen diffraction-plane detector is typically recorded as a function of scan position. (c) Dynamic hollow-cone illumination (DHCI) TEM which is the same as (a) except the illumination is precessed in a hollow-cone during image acquisition.

an imaging mode less susceptible to coherent interference effects of the electron wave, reducing the effects of dynamical diffraction (Rebled et al., 2011) or making crystalline nano-objects and stained biological samples more visible against a background of an amorphous support material (Kunath et al., 1985; Nagata et al., 1976). Another technique of note is "imaging" STEM (Rosenauer et al., 2014) where an incoherent illumination condition is achieved by integrating the TEM image formed during the scan of a focused electron probe across the field of view. The DHCI TEM technique can be considered the imaging analogy to precession electron diffraction (PED) (Vincent & Midgley, 1994; Avilov et al., 2007), a successful structural determination technique for nanostructures which produces diffraction patterns considered pseudo-kinematical, meaning the effects of multiple electron scattering ~~is~~ are diminished in the resulting diffraction patterns (Ciston et al., 2008) and structural determination from these experimental results is more straight-forward. Consequently we also expect the effects of multiple electron scattering to be somewhat reduced in DHCI TEM imaging so that a more consistent TEM image result is achieved for different thicknesses of the same crystal.

We note the similarity of DHCI TEM technique to ABF STEM ~~STEM-ABF~~ via reciprocity, see Fig. 1. In electron microscopy reciprocity implies that CTEM and STEM experiments will produce equivalent results if a point-like STEM detector and the tilt vector of the CTEM illumination are at the same positions in reciprocal space and an equivalent electron lens is used in both experiments (Pogany & Turner, 1968; Cowley, 1969). The CTEM illumination equivalent of a finite size STEM detector is illumination that incoherently fills the reciprocal space area of the equivalent STEM detector. For example equivalent results to STEM-ABF have been achieved in the imaging STEM technique using a scanned hollow-cone illumination that matched the outer angle of the image forming lens objective (Rosenauer et al., 2014). Thus the STEM equivalent of DHCI TEM is STEM with a thin ring detector and, if the hollow-cone semi angle of the DHCI illumination is chosen to be just less than the radius of the CTEM objective aperture, the DHCI technique should produce results that are similar to ABF STEM ~~STEM-ABF~~ (Ishikawa et al., 2011). Equivalent results would eventuate if the DHCI illumination were precessed through a "solid" range of angles that filled the annular detector employed in the STEM experiment rather than a "hollow" cone that is equivalent to a very thin "ring" detector. This would be expected to translate some of the benefits of ABF STEM ~~STEM-ABF~~ imaging, notably an imaging mode that allows identification of light and heavy atoms and is also robust to multiple electron scattering in thick crystalline samples. We note that this proposed method of DHCI-TEM differs subtley from the that which was typically implemented in the past. Previous investigations assumed a microscope without spherical aberration correction and the phase curvature imparted onto the electron wave by the aberrated lens was an important part of the phase contrast mechanism. By blocking a component of the scattered electron beam as it is precessed about the optic axis the aperture acts acts as an alternative phase contrast mechanism [this

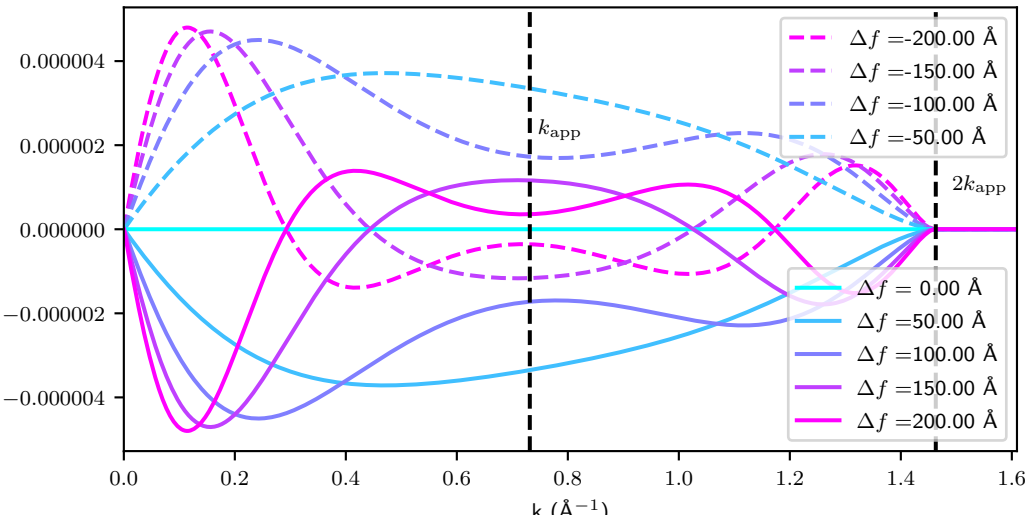

Figure 2: The phase contrast transfer function (PCTF) for DCHI-TEM as implemented in this manuscript for a number of different defocus values. An objective aperture of 14.4 mrad, probe accelerating voltage of 300 keV and no lens aberrations aside from defocus are assumed. Information transfer up to twice the reciprocal space radius of the probe forming aperture is possible and there is effective transfer of long range spatial frequencies for larger defocii.

is analagous to Schleiren or Foucault knife-edge optics (Nagayama et al., 2010)] though the ultimate aim of using an objective aperture is to emulate ABF STEM. More recently Ishikawa et al. (2011) presented DHCI-TEM contrast transfer functions for a corrected instrument but with the assumption that residual fifth order spherical aberration, not an aperture, provides contrast. Shown in Fig.2 are calculated CTFs for a hollowcone imaging assuming a precession cone and objective aperture of 14.4 mrad for a 300 keV probe. Similar to ABF STEM (Seki et al., 2018), the contrast transfer band for DHCI-TEM is negative for overfocus ($\Delta f > 0$), positive for underfocus ($\Delta f < 0$) and zero for the case of $\Delta f = 0$ Å. Similar to ABF STEM (Seki et al., 2018), for atomic resolution imaging of thick specimens with a probe focussed on the surface of the specimen we therefore expect that atomic columns will appear black since the probe will be displaced in the negative z direction with respect to the atoms. For small defocii ($\Delta f \leq 100$ Å), the frequency pass band is smooth with little fluctuation. Reasonable information transfer is predicted up to twice the aperture limit and, especially for large defocii, the information transfer of low spatial frequencies is very favourable. This is a feature of Shleiren optical systems which have been used in electron microscopy to visualize "topographical contrast": the often difficult to see long-range phase modulation in samples (Cullis & Maher, 1975).

Since STEM-ABF is sensitive to the alignment of detector, probe forming aperture and specimen zone axis (Findlay et al., 2010; Zhou et al., 2016; Brown et al., 2017) we also expect, and will demonstrate in simulation, that DHCI-TEM can be difficult in practice as it is sensitive to the alignment of precession axis, microscope objective aperture and crystal zone axis. This is consistent with earlier explorations of the technique, where even misalignments of the illumination cone and the optic axis smaller than a milliradian were detectable (Kunath et al., 1985)

In this paper we demonstrate imaging of light and heavy atoms simultaneously in DHCI-TEM in experiment and explore its benefits and demonstrate its sensitivity to misalignment in simulation.

2 Materials and methods

For the experimental results a $SrTiO_3$ lamella, a material chosen for its availabity of heavy (Sr and Ti) and light (O) atoms, was prepared using a focused ion beam instrument. The TEM sample was prepared by the FIB liftout technique with final thinning performed with the Ga+ beam at 0.5 kV. ~~Imaging was performed in an image spherical aberration (C_S) corrected Thermo Fisher Titan Themis instrument operated at 300 kV. Since the use of an objective lens was anticipated, the image corrector was aligned with a 50 micron objective (measured to have a radius of approximately 0.74 Å^{-1} or 14.4 mrad for 300 kV electrons) inserted to balance the significant two-fold astigmatism, and likely other aberrations, that resulted from the insertion of the aperture strip. This additional astigmatism was thought to be a result of pertubation of the fringing fields for the objective lens pole piece by the aperture strip.~~ Imaging was performed in an image spherical aberration (CS)

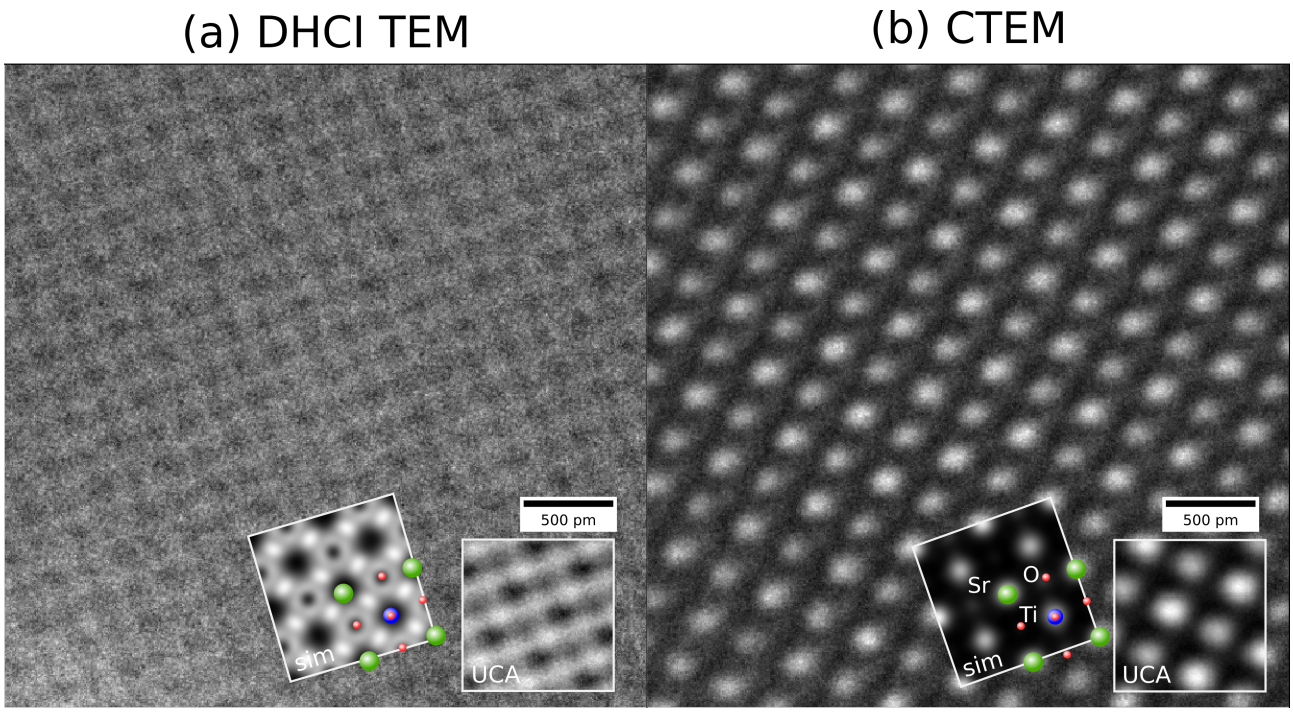

Figure 3: (a) DHCI and (b) CTEM images of a similar region in the $SrTiO_3$ crystal with unit cell averages (UCA) and corresponding simulations (sim) inset (assuming a specimen thickness of 700 Å and defocii of 0 Å and -300 Å for DHCI and CTEM respectively). A reduction in contrast is visible in the DHCI TEM image in (a) compared to the CTEM image in (b), consistent with previously reported results (Geipel & Mader, 1996). However, the DHCI TEM image in (a) enables identification of the O columns, which is not possible for this particular combination of specimen thickness and lens defocus in the CTEM image in (b).

corrected Thermo Fisher Titan Themis instrument operated at 300 kV. An objective aperture is required to provide interpretable contrast in DHCI-TEM in approximate reciprocity to ABF STEM. The insertion of an objective aperture leads to significant two-fold astigmatism, and likely other aberrations, thought to be a result of perturbation of the fringing fields for the objective lens pole piece by the aperture strip. Consequently, the image corrector was aligned with a 50 micron objective inserted (measured to have a radius of approximately 0.74 $Å^{-1}$ or 14.4 mrad for 300 kV electrons) to correct for any unavoidable residual aberrations that would be introduced by this necessary aperture. Alignment of the image corrector with the aperture strip inserted significantly constrained the maximum tilt angle possible for the Zemlin tableau method of fitting aberrations (since a beam with a large tilt angle would be blocked by the objective). This meant that the ability of the software to accurately characterise and compensate for small higher order aberrations ~~were~~ was limited and we were only able to achieve a ronchigram where the deviation in the phase was less than $\pi/4$ out to about 12 mrad. A flat phase region meeting the $\pi/4$ criterion out to 25-30 mrad is usually achieved in more conventional operation of this particular instrument.

The $SrTiO_3$ specimen was aligned down its [001] axis and beam precession was performed using the "dynamic dark field" option in the microscope software interface. Maximum precession frequency of this mode is around 10 Hz [1] and no instabilities of cone eccentricity, angle or precession frequency where noticeable. Precise alignment of the so-called dynamic beam-tilt pivot points, which ensure that the real-space position of the beam on the sample was maintained whilst the beam is precessed through a range of tilt angles, was necessary.

For simulated results a multislice method using software written in the Python language and using the PyTorch library[2] for GPU acceleration. The source code is attached in the supplementary materials.

3 Results and Discussion

Images of a region of the $SrTiO_3$ crystal are shown in Fig. 3 both in DHCI TEM mode and ~~the more conventional~~ CTEM mode. Inset within these images are the unit-cell-averages for the region, to improve signal to noise of the image, and corresponding simulations. For the simulation assuming a 700 Å thick sample and defocii of 0 Å, for the DHCI-TEM image, and 300 Å, for the CTEM image, (-negative defocus is taken to be underfocus, with the

[1] Precession frequencies in the kHz range are possible with specialist modifications of a TEM instrument (Own et al., 2005), now commercially available as a plugin system for most TEMs, see https://www.nanomegas.com/.

[2] https://pytorch.org/

focal point being inside the the specimen and zero defocus as being the lens focused on the specimen exit surface) provided a reasonable match with the experiment. Since we are only interested in a qualitative match between theory and experiment for discussion of the merits of the different TEM approaches no attempt was made to account for resolution-degrading experimental effects such as camera modulation transfer function (MTF) or chromatic aberration and we note that for the CTEM images the absolute defocus value is ambiguous. Most importantly, the precession TEM result allows direct identification of the all of the Sr, Ti and O columns from the data at the cost of reduced signal to noise, the latter effect being consistent with previous results (Geipel & Mader, 1996). It should be stressed that to be able to observe the O columns the concentric alignment of objective aperture, tilt precession cone and specimen zone axis had to be extremely precise. The images shown are from a 3.6 nm × 3.6 nm region cropped from a total 28.6 nm × 28.6 nm field of view. ~~and~~ Shifts in the apparent positions of the O columns due to misalignment of the sample zone axis ~~due to the~~ resulting from specimen bending are visible across ~~this~~ the larger 28.6 nm × 28.6 nm field of view .~~,~~ An example ~~of which are displayed~~ misaligned region is included in Fig. S 1 of the supplementary materials.

To observe the benefits of the DHCI technique as compared to ~~conventional bright-field~~ CTEM for a wider range of experimental parameters defocus thickness montages were simulated and are shown in Fig. 4 for a 300 kV electron probe and 14.4 mrad aperture, consistent with experiment. DHCI TEM are displayed in Fig. 4 (a) and CTEM images in Fig. 4(b). Annular bright-field (ABF) STEM images are also shown in Fig. 4(c) for comparison, and the similarity with DHCI TEM in Fig. 4(a) is clear. The defocus-thickness montage for ~~conventional bright-field~~ CTEM images which demonstrates some of the challenges in using the technique. What appear to be atomic columns are evident for a defocus close to zero but also around 400 Å for most of the thicknesses in the series. Furthermore, the interpretation of these apparent columns is ambiguous, for a defocus of around 0 Å the appearance of atomic columns corresponds to pure O columns, but for a focus of around 400 Å peaks in intensity that give the appearance of atomic columns~~columns visible in the image~~ correpond to the Sr and Ti-O columns. The DHCI TEM images shown in Fig. 4(a) allow for easier interpretation. For the lens focused on the surface of the material (our defocus convention for STEM is that a probe with defocus < 0 would converge inside the specimen) black dots correspond to the positions of the Sr, Ti-O and O columns, as is the case in the ABF STEM images in Fig. 4(c). The contrast at this defocus value for DHCI-TEM is typically distinct from the other defocii, making it a relatively straight-forward focal plane to find in experiment. This can be seen by inspection of the montage in Fig. 4(a) and but is also shown in the corresponding plot of contrast vs. defocus for a subset of the thicknesses in the montage in Fig. 4(d). A simulated DHCI-TEM montage, identical to Fig. 4(a) but for the fact that no objective aperture was assumed, is displayed in Fig. S 2 of the supplementary materials. This montage demonstrates the importance of the objective aperture in obtaining ABF STEM like contrast since the plane of directly interpretable contrast in Fig. 4(a) is observed to disappear in Fig. S 2 of the supplementary materials nor is there a plane where contrast appears to be maximized. The equivalent contrast vs. defocus plot for CTEM in Fig. 4(e) shows that maximum contrast only occasionally corresponds to the lens being focused on the exit surface of the crystal (the zero defocus case) and that maximum contrast can appear at any number of defocii[3]. We re-emphasize that there is only a loose equivalence between DHCI-TEM and ABF-STEM that does not amount to strict fulfillment of the conditions for TEM-STEM reciprocity. Reciprocity requires that the angular range of the detector in ABF STEM and the reciprocal space area of precession in DHCI-TEM to be equivalent (Ishikawa et al., 2011). Therefore, as implemented in this paper, whilst both imaging methods produce intensity minima (black dots) that correspond to atomic columns at zero defocus, for many defocii and thicknesses these imaging methods do not agree. For example, a defocus of 300 Å for a specimen thickness of 500 Å produces intensity maxima at the O column positions in DHCI-TEM but not in ABF-STEM.

Simulations also allow us to more systematically explore the sensitivity of the DHCI TEM technique to alignment issues. In Fig. 5 simulated DHCI TEM images of 200 Å and 700 Å thick $SrTiO~~3~~_3$ with just a few mrad misalignment of either the hollow-cone illumination or the specimen zone axis with the microscope's optic axis. Misalignment of just 1 mrad of either the illumination or zone axis produces noticable results, particularly for the thicker 700 Å sample. As is the case for ABF STEM ~~STEM ABF~~ (Findlay et al., 2010; Zhou et al., 2016; Brown et al., 2017), the light atomic columns shift more than do the heavy atomic columns, and in some cases, particularly the 3 mrad misalignemnt of either the illumination or zone axis for the 700 Å case, the O atomic columns are no longer recognisable. These results are consistent with the alignment sensitivity that was observed in experiment.

Given the trade-off between image contrast and interpretability that seems inherent in the DHCI TEM technique it is worth discussing future innovations in TEM methods. Authors have pointed out that the ABF STEM ~~STEM ABF~~ technique is quite an inefficient way of producing phase constrast and the advent of fast readout pixelated detectors in STEM, a technique often referred to as 4D-STEM, offer more efficient alternatives such as ptycography and differential phase contrast (DPC) STEM (Pennycook et al., 2015). By

[3]the reader should bear in mind that these simulations do not take into account partial coherence in the electron beam and that these oscillations in contrast are unlikely to continue indefinitely

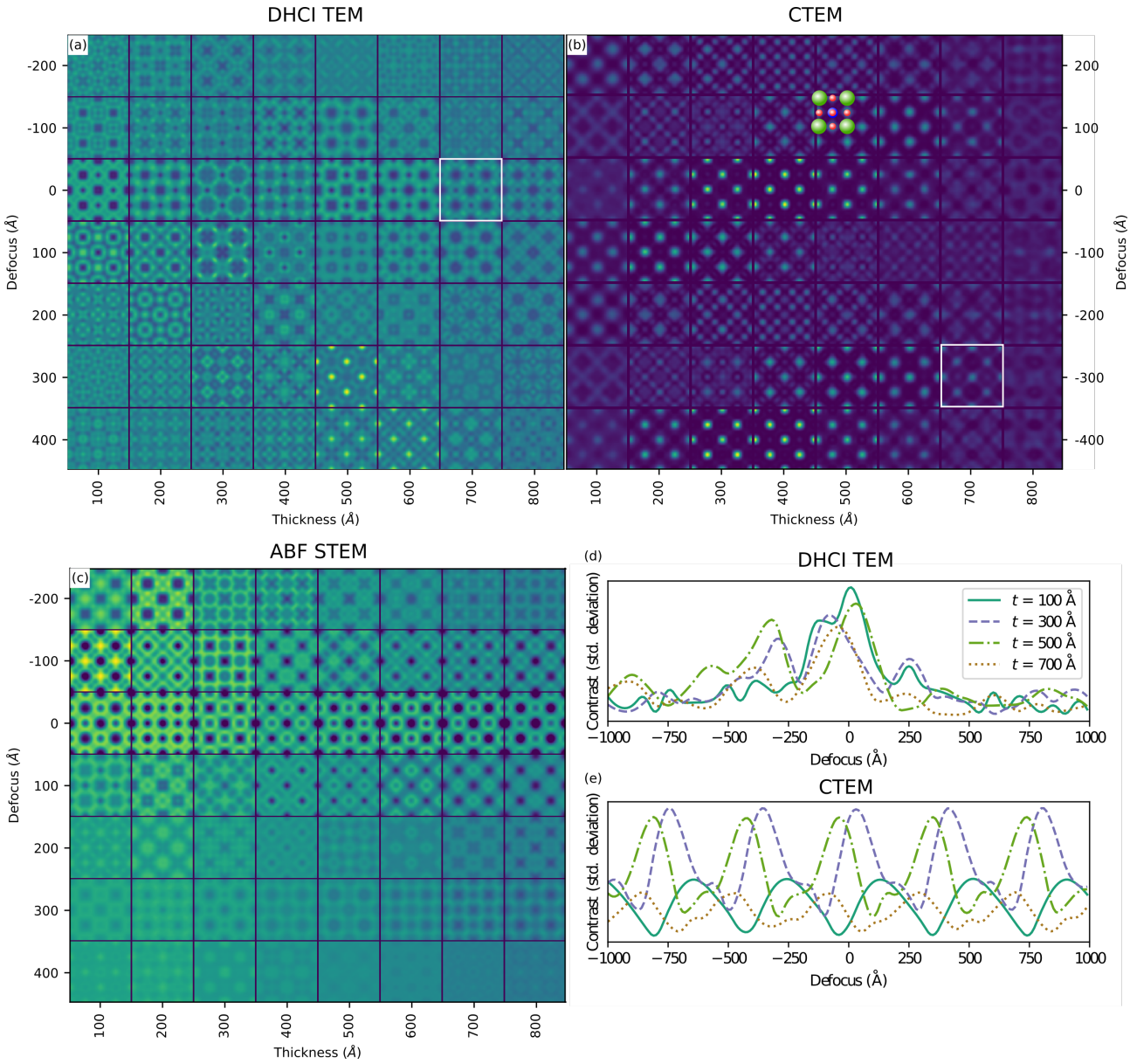

Figure 4: Thickness-defocus montages for (a) DHCI TEM, (b) ~~bright-field~~ CTEM images and (c) annular bright-field (ABF) STEM for an 001 oriented $SrTiO~~3~~_3$ crystal. Highlight squares in (a) and (b) indicate the simulations that were displayed in Fig. 3. For the ~~bright-field~~ CTEM images, there are no simple relationships between image contrast and column position location that hold for a wide range of thicknesses and defocii. In the zero focus condition for DHCI TEM and ABF STEM images black dots always correspond to column locations. Also shown are plots of the contrast (as measured by the standard deviation metric) vs. defocus for a subset of the thicknesses but a larger range of defocii for (d) DHCI-TEM and (e) CTEM , maximum contrast is typically achieved for DHCI TEM for a defocus of around 0 Å, whilst in CTEM maximum contrast can be commonly achieved even for large defocii (partial coherence would likely affect this in experiment).

analogy the DHCI TEM imaging method exhibits a similar inefficiency as compared to CTEM. Recently datasets equivalent to 4D-STEM have been produced by recording TEM images for a set of tilts of the plane-wave illumination (Barnum, 2019) meaning that ptychographic and DPC approaches might be extended to ~~conventional bright-field~~ CTEM experiments. With technology available today synchronization of computer controlled beam tilt with fast-readout electron cameras and live processing of these results could produce images with real-time frame rates (frame rates > 50 Hz or so), for more robust and interpretable phase contrast and wide fields of view. Proof of principle research into this suggested technique would elucidate the best processing methods that could be applied to these datasets and would be the logical next step in investigations.

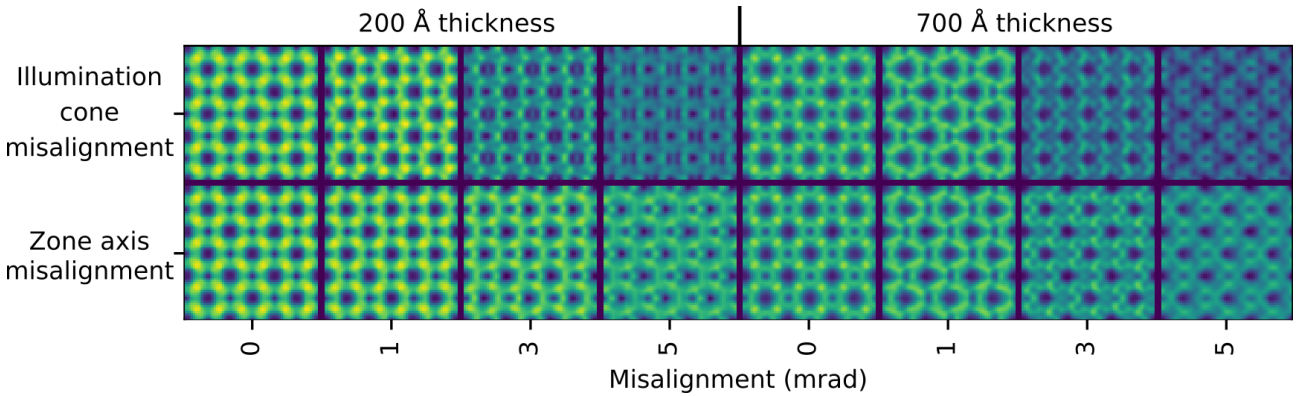

Figure 5: The effect of different amounts of misalignment in mrad of the dynamic hollow-cone illumination or the specimen zone-axis on a DHCI-TEM image of a $SrTiO_3$ crystal for different thicknesses of 200 Å and 700 Å.

4 Conclusions

We have experimentally demonstrated the ability of DHCI-TEM to form more directly interpretable maps of light atomic columns in a crystalline environment, at the cost of reduced contrast. The precise concentric alignment of the specimen zone-axis and the tilt cone with the specimen zone axis mean that this technique is challenging in its application.

5 Acknowledgements

Work at the Molecular Foundry was supported by the Office of Science, Office of Basic Energy Sciences, of the U.S. Department of Energy under Contract No. DE-AC02-05CH11231. HGB and JC acknowledge additional support from the Presidential Early Career Award for Scientists and Engineers (PECASE) through the U.S. Department of Energy. The authors acknowledge sample preparation support from Thermo Fisher Scientific. Helpful discussions with Dr. Alex Eggeman of the University of Manchester are also acknowledged.

6 References

References

Avilov, A., Kuligin, K., Nicolopoulos, S., Nickolskiy, M., Boulahya, K., Portillo, J., Lepeshov, G., Sobolev, B., Collette, J.P., Martin, N., Robins, A.C. & Fischione, P. (2007). Precession technique and electron diffractometry as new tools for crystal structure analysis and chemical bonding determination, *Ultramicroscopy* **107**, 431–444.

Barnum, A. (2019). k-scanning: An alternative to 4D-STEM, *Microscopy and Microanalysis* **25**, 1932–1933.

Brown, H.G., Ishikawa, R., Sánchez-Santolino, G., Lugg, N.R., Ikuhara, Y., Allen, L.J. & Shibata, N. (2017). A new method to detect and correct sample tilt in scanning transmission electron microscopy bright-field imaging, *Ultramicroscopy* **173**, 76–83.

Ciston, J., Deng, B., Marks, L.D., Own, C.S. & Sinkler, W. (2008). A quantitative analysis of the cone-angle dependence in precession electron diffraction, *Ultramicroscopy* **108**, 514–522.

Cowley, J.M. (1969). Image contrast in a transmission scanning electron microscope, *Applied Physics Letters* **15**, 58–59.

Cowley, J.M. & Moodie, A.F. (1957). Fourier images: I-the point source, *Proceedings of the Physical Society Section B* **70**, 486.

Cullis, A. & Maher, D. (1975). Topographical contrast in the transmission electron microscope, *Ultramicroscopy* **1**, 97–112.

Findlay, S.D., Shibata, N., Sawada, H., Okunishi, E., Kondo, Y. & Ikuhara, Y. (2010). Dynamics of annular bright field imaging in scanning transmission electron microscopy, *Ultramicroscopy* **110**, 903–923.

Findlay, S.D., Shibata, N., Sawada, H., Okunishi, E., Kondo, Y., Yamamoto, T. & Ikuhara, Y. (2009). Robust atomic resolution imaging of light elements using scanning transmission electron microscopy, *Applied Physics Letters* **95**, 191913.

Geipel, T. & Mader, W. (1996). Practical aspects of hollow-cone imaging, *Ultramicroscopy* **63**, 65–74.

Henderson, R. (1995). The potential and limitations of neutrons, electrons and x-rays for atomic resolution microscopy of unstained biological molecules, *Quarterly reviews of biophysics* **28**, 171–193.

Ishikawa, R., Okunishi, E., Sawada, H., Kondo, Y., Hosokawa, F. & Abe, E. (2011). Direct imaging of hydrogen-atom columns in a crystal by annular bright-field electron microscopy, *Nature materials* **10**, 278–281.

Kunath, W., Zemlin, F. & Weiss, K. (1985). Apodization in phase-contrast electron microscopy realized with hollow-cone illumination, *Ultramicroscopy* **16**, 123–138.

Nagata, F., Matsuda, T., Komoda, T. & Hama, K. (1976). High resolution observation of biological specimens by an incoherent illumination method, *Microscopy* **25**, 237–243.

Nagayama, K., Danev, R., Shigematsu, H., Hosogi, N., Fukuda, Y., Nitta, K. & Kaneko, Y. (2010). Phase contrast enhancement with phase plates in biological electron microscopy, *Microscopy Today* **18**, 10–13.

Own, C., Marks, L. & Sinkler, W. (2005). Electron precession: A guide for implementation, *Review of Scientific Instruments* **76**, 033703.

Pennycook, S.J. & Boatner, L.A. (1988). Chemically sensitive structure-imaging with a scanning transmission electron microscope, *Nature* **336**, 565.

Pennycook, T.J., Lupini, A.R., Yang, H., Murfitt, M.F., Jones, L. & Nellist, P.D. (2015). Efficient phase contrast imaging in stem using a pixelated detector. part 1: Experimental demonstration at atomic resolution, *Ultramicroscopy* **151**, 160–167.

Pogany, A.P. & Turner, P.S. (1968). Reciprocity in electron diffraction and microscopy, *Acta Crystallographica Section A: Crystal Physics, Diffraction, Theoretical and General Crystallography* **24**, 103–109.

Rebled, J.M., Yedra, L.l., Estrade, S., Portillo, J. & Peiro, F. (2011). A new approach for 3D reconstruction from bright field tem imaging: beam precession assisted electron tomography, *Ultramicroscopy* **111**, 1504–1511.

Rez, P. (2003). Comparison of phase contrast transmission electron microscopy with optimized scanning transmission annular dark field imaging for protein imaging, *Ultramicroscopy* **96**, 117–124.

Rosenauer, A., Krause, F.F., Müller, K., Schowalter, M. & Mehrtens, T. (2014). Conventional transmission electron microscopy imaging beyond the diffraction and information limits, *Physical review letters* **113**, 096101.

Saxton, W.O., Jenkins, W.K., Freeman, L.A. & Smith, D. (1978). Tem observations using bright field hollow cone illumination., *Optik (Jena)* **49**, 505–510.

Seki, T., Takanashi, N. & Abe, E. (2018). Integrated contrast-transfer-function for aberration-corrected phase-contrast stem, *Ultramicroscopy* **194**, 193–198.

Sidorov, M.V., McCartney, M.R. & Smith, D.J. (2000). High resolution TEM imaging with hollow-cone illumination, *Microscopy And Microanalysis* **3**, 1191–1192.

Spence, J.C.H. (2013). *High-resolution electron microscopy*, chap. 5, 121–191, OUP Oxford.

Vincent, R. & Midgley, P.A. (1994). Double conical beam-rocking system for measurement of integrated electron diffraction intensities, *Ultramicroscopy* **53**, 271–282.

Zhou, D., Müller-Caspary, K., Sigle, W., Krause, F.F., Rosenauer, A. & van Aken, P.A. (2016). Sample tilt effects on atom column position determination in ABF–STEM imaging, *Ultramicroscopy* **160**, 110–117.